Journal of The Electrochemical Society, **162** (14) H922-H928 (2015)
0013-4651/2015/162(14)/H922/7/$33.00 © The Electrochemical Society

High-Performance Gel-Type Dye-Sensitized Solar Cells Using Poly (methyl methacrylate-*co*-ethylacrylate)-Based Polymer Gel Electrolyte with Superior Enduring Stability

Zahra Seidalilir,[a] Rasoul Malekfar,[a,z] Jia-Wei Shiu,[b] Hui-Ping Wu,[b] and Eric Wei-Guang Diau[b,z]

[a]*Atomic and Molecular Group, Physics Department, Tarbait Modares University, 1411713116 Tehran, Iran*
[b]*Department of Applied Chemistry and Institute of Molecular Science, National Chiao Tung University, Hsinchu 30010, Taiwan*

We fabricated high-performance gel-state dye-sensitized solar cells (DSSCs) using TiO_2 nanoparticles (NPs) and one-dimensional TiO_2 nanotube (NT) arrays as electrodes and a polymer gel electrolyte (PGE), poly(methyl methacrylate-co-ethyl acrylate) (PMMA-EA), as a gelator in 3-methoxypropionitrile (MPN). MPN instead of acetonitrile (ACN) was used as a solvent to prepare PGE to overcome the drawback of high volatility of ACN so as to improve the long-term stability of the devices. The viscosities of the PGEs containing varied concentrations of PMMA-EA copolymer (4–13 wt%) were measured to obtain the gel to liquid phase transition temperature (T_p) of the PGEs. T_p systematically increased with increasing concentration of PMMA-EA. We found that the as prepared PGE showed the best electrical conductivity of 1.6 mS cm^{-1} at 10 wt% of PMMA-EA, which is comparable with the value of the liquid electrolyte (1.7 mS cm^{-1}). By employing 10 wt% of PMMA-EA as PGE in MPN, the gel-type NT and NP-based devices exhibited power conversion efficiencies (PCE) 6.3 and 8.4%, respectively, which are comparable to those of the corresponding liquid-type counterparts, PCE = 6.4 and 9.1%, respectively. In addition, the enduring stability of MPN-based gel-state device was found to retain a high device efficiency for a long period under thermal and light-soaking dual stress.
 [DOI: 10.1149/2.0611514jes]

Manuscript received September 3, 2015. Published October 9, 2015.

Dye-sensitized solar cells (DSSCs) have received considerable attention in recent years because they are promising next-generation photovoltaic devices alternative to conventional Si-based solar cells.[1] A conventional DSSC made of an electron collecting layer composed of randomly interconnected TiO_2 nanoparticles (NPs), dyes, liquid electrolytes, and a counter electrode.[2] However, the high-performance DSSC devices fabricated with liquid-type electrolyte suffered from leakage and volatilization of the liquid solvent, and serious problems might arise when the devices were imposed under light soaking and thermal stress conditions.[3] To solve the problems for the enduring instability of these traditional liquid-type DSSCs, solid-state or quasi-solid-state electrolytes, such as organic hole-transport materials,[4] p-type inorganic semiconductors,[5] gel-electrolytes incorporating redox couples[6] and ionic liquid electrolytes[7] were used instead of liquid electrolytes. However, solid-state DSSCs exhibited lower conversion efficiency compared to their liquid-type counterparts due to the poor ionic conductivity and lower ion diffusion.[8] To enhance the thermal stability of the devices at the same time also maintain a great ionic conductivity for the electrolytes, varied quasi solid state electrolytes have been utilized, such as polymer gel electrolytes (PGEs) in which both liquid and solid phases are combined.

In a PGE, the liquid electrolyte was trapped in a three dimensional network including polymer cages which was provided by polymer host, thereby, the solvent evaporation was inhibited, which has been proven to improve the long-term stability of DSSCs.[9] Pure polymers like poly (ethylene glycol) (PEG),[10] poly (acrylonitrile) (PAN)[11] and poly (methyl methacrylate) (PMMA)[12] have been used as gelators to prepare PGEs for DSSC applications. On the other hand, the solubility of these polymers in ACN or MPN might become a problem. The strategy to solve this problem is to use the approach of copolymerization for which the side chains of the copolymer improve the solubility while the main polymer chain can still form great polymeric network for enhanced ionic conductivity. The most promising examples for the copolymer gel electrolyte systems include poly (vinylidene fluoride-co-hexafluoropropylene) (PVDF–HFP),[13] poly (methyl methacrylate-co-acrylonitrile) (PMMA-AN)[14] and poly (acrylonitrile-co-vinyl acetate) (PAN–VA).[15]

On the other hand, it has been pointed out that NP-based DSSC made of N719 dye suffered from dye desorption at high temperature (80°C) even using copolymer PVDF-HFP as a gel electrolyte.[3] However, when the amphiphilic ruthenium sensitizer Z907 dye[16] was implemented, the PGE-based device can sustain PCE 6.0% for 1000 h at 80°C in the dark.[3] This is a very important step for DSSC with great thermal stability matching the standard of a silicon-based solar cell. Further development based on the PAN-VA electrolyte using CYC-B11 dye was reported to attain PCE exceeding 10% under one sun of irradiation,[15] but the PGE with 7 wt% PAN-VA encountered a problem of solvent (ACN) evaporation under light-soaking examination at 60°C. Therefore, it is always a challenge to fabricate a highly efficient DSSC with superior enduring performance stability under severe conditions of light soaking and thermal stress.

Even though the gel-type device sensitized with the amphiphilic Z907 dye exhibited remarkable performance stability under an extensive thermal stress condition,[3] the small absorptivity of the dye limits the device performance to compete with other heteroleptic ruthenium dyes.[15,17–19] Recently we have demonstrated that the performance of the Z907 device can be significantly improved to reach PCE 10% upon sophisticated structural engineering for the hybrid TiO_2 films with a bi-layer or a multi-layer configuration.[20–22] Moreover, we showed that the performance of the Z907 device with an ACN-based liquid-type electrolyte can be optimized to reach PCE 10.2% and maintained this performance in the dark for at least 1000 h.[22] Further light-soaking test of the same device showed only a slight performance degradation under thermal stress performing at 60–70°C, but the performance degraded significantly and rapidly when the device temperature was increased to 80°C under one-sun irradiation because the evaporation of the acetonitrile (ACN) solvent occurred quickly at 80°C.[22]

ACN and 3-methoxypropionitrile (MPN) are the two major types of organic solvents which usually used to prepare liquid electrolytes for DSSC applications. Gel-state DSSCs using ACN as a solvent showed superior power conversion efficiency (PCE) compared to those based on other solvents. However, high volatility of ACN leads to a lower gel to liquid phase transition temperature (T_p) for the PGEs and therefore limits the long-term stability of the gel-state devices. To overcome this problem, MPN, which has a higher boiling point and lower volatility than those of ACN, was utilized as the solvent to increase phase transition temperature of PGEs. Therefore, the long-term stability of the MPN-based gel-state device can be further improved.[23]

The relatively poor performance of gel-state DSSCs based on NP layers as photoanode might be associated with the following two

[z]E-mail: malekfar@modares.ac.ir; diau@mail.nctu.edu.tw

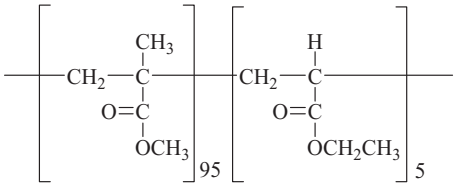

Chart 1. Molecular structure of poly (methyl methacrylate-co-ethylacrylate) (PMMA–EA) with a mean molar mass of 101000 g mol^{-1}.

challenges: (1) limited pore filling of the mesoporous TiO_2 photoelectrodes containing NP layers with viscous polymer gel electrolytes;[24] (2) trap limited diffusion for electron transport in randomly packed TiO_2 NPs.[25] Therefore, structural modification of TiO_2 is encouraged in order to develop high-performance gel-state DSSCs. For example, one-dimensional (1D) TiO_2 nanostructures such as nanotube arrays are suitable alternatives as a photoanode for DSSC to enhance the charge-collection efficiency by promoting faster transport and slower recombination.[26] The use of TiO_2 nanotubes (TiNTs) as the photoanode for fabrication of liquid-state DSSCs has been performed by several groups.[27–31] To increase the interfacial contact between TiO_2 nanostructures and the electrolyte as well as to improve the ability of charge transport, TiNTs have been used as an efficient photoanode for all-solid-state DSSCs.[32–34]

To overcome the problem for the enduring stability of the device beyond 80°C, in the present study we further applied the concept of PGE to fabricate the gel-state NP-based DSSC using Z907 dye with the goal to enable DSSC featuring both extraordinary long-term stability and great device performance for commercialization. Recently we have fabricated gel-state NT-DSSCs using N719 dye and PGE containing PMMA-EA copolymer in ACN solvent.[35] We demonstrated that the performance of the device using PGE containing 7 wt% of PMMA-EA can be optimized to reach PCE 6.9%, which was comparable with that of a corresponding liquid-type device, PCE = 7.1% and maintained ∼90% of this performance after 1000 h under one-sun illumination at 50°C. PMMA was selected as a gelling agent because it can form gel state in a suitable concentration with great ionic conductivity.[12] The proposed PGE system composes of the polymer chain PMMA with 5% of ethyl acrylate (EA) (PMMA-EA, the molecular structure is shown in Chart 1) to prevent unzipping of the polymer at elevated temperatures; the ester groups in the copolymer PMMA-EA would capture appropriate amount of solvent within its polymeric chain structure and form a loose elastomeric network in the gel state.[36,37] Herein varied portions of PMMA-EA (4–13 wt%) were added to a MPN-based liquid-type electrolyte to form PGEs for the gel-state N719-based NT-DSSCs (NT/N719 system) and Z907-based devices fabricated with the best-performing hybrid TiO_2 nanoparticle films with a bilayer configuration (NP/Z907 system). The 1D structure of TiNTs offers great charge transport features and their open structures improve light harvesting efficiency and also help on the penetration of gel-state electrolyte. The best performance of the NT-DSSC devices using an ACN-based liquid redox electrolyte and N719 dye was achieved at tube length ∼30 μm for a device structure under rear illumination.[28,29] Therefore, we used TiNT arrays with tube length ∼30 μm to fabricate MPN-based gel-state NT-DSSCs. We optimized the concentrations of PMMA-EA in MPN to obtain the best gel-state DSSC performance for both NT/N719 and NP/Z907 systems. The aims of using MPN-based PGE in both NT/N719 and NP/Z907 devices are to attain the best PCE for NT and NP based DSSCs and also improve enduring stability of gel-state devices. Overall PCEs 6.3 and 8.4% have been successfully achieved for gel-state NT/N719 and NP/Z907 devices, respectively, by using the new PGE containing 10 wt% of PMMA-EA in MPN, which were 98 and 92% of the performance of the corresponding liquid-type devices, respectively. The long-term stability examinations indicate that the NP/Z907 device made of 7 wt% PMMA-EA in the ACN-based PGE was endurable at 80°C with PCE greater than 8.0% under one-sun illumination whereas the device made of 10 wt% PMMA-EA in the MPN-based PGE was endurable even at 85°C with PCE exceeding 7.5% under one-sun illumination. This is the first example demonstrating a promising feature for a gel-type DSSC to sustain a high device performance for a long period under extreme thermal stress and light-soaking conditions that matched the durability criteria applied to silicon solar cells for outdoor applications.

Experimental

Fabrication of TiNT arrays.— Ordered TiNT arrays were fabricated using a potentiostatic anodization in a two-electrodes electrochemical cell[27,28] where Ti foil (commercially pure grade1, purity 99.9%, substrate size 6 × 6 cm^2, thickness 130 μm, Kobe Steel) was the anode to grow TiNT arrays on it and another Ti foil with the same size was the cathode and the two electrodes with a fixed interval of 2.7 cm were placed in a thermostatic container (T = 22°C), containing the electrolyte solution for anodization. Preparation of the ordered TiNT arrays with L = 30 μm was performed using electrolyte solutions containing NH_4F (purity 99.9%, 0.4 wt%) in ethylene glycol in the presence of H_2O (2 vol %) at 60 V for 12 h. Then the anodic sample was washed in ethanol, and annealed at 450°C for 1 h to convert the amorphous TiO_2 into its anatase phase. The annealed sample was then ultrasonicated in ethanol for 15 min to remove unwanted deposits on the TiNT surface introduced through anodization.[28,29] To enhance the effective surface area of the tubes for dye adsorption and thus improve cell performance, the as prepared TiNT films were immersed in $TiCl_4$ solution (0.073 M, 30 min) and then washed and dried near 50°C. The films were treated again with fresh $TiCl_4$ aqueous solution for 2 h and sintered at 350°C for 30 min. The surface morphology of the TiNT films was determined using a scanning electron microscope (SEM, JSM-6390LV, JEOL).

Preparation of electrolytes.— PGEs were prepared with PMMA-EA (Aldrich, mean molar mass 101000 g mol^{-1}, ethyl acrylate concentration < 5 wt%) mixed with the liquid electrolyte containing 0.05 M lithium iodide (LiI), 0.03 M diiodine (I_2), 0.5 M 4-tert-butylpyridine (TBP), 1.0 M 1-methyl-3-propylimidazolium iodide (PMII) and 0.1 M guanidinium thiocyanate (GuNCS) in MPN with weight percentages of 4, 7, 10 and 13. Then the mixtures were heated along with stirring at 70°C until homogeneous viscous solutions were obtained. PMMA-EA is very soluble in the MPN-based liquid electrolyte, forming a liquid-state polymer electrolyte which the cells can be conveniently filled with the as prepared electrolytes. At the room temperature condition, the liquid-state polymer electrolyte solution converts to the gel-state electrolyte over a period of days. However, the gelation time can be decreased significantly by cooling. To obtain phase transition temperature of the PGEs, thermal dependence of the viscosities of the electrolytes was investigated using a programmable rheometer (DV-III, Brookfield).

Device fabrication.— A paste composed of TiO_2 nanoparticles (particle size ∼20 nm) was prepared using a normal combined sol-gel/hydrothermal method.[20] The TiO_2 paste was then coated on a $TiCl_4$-pretreated fluorine-doped tin oxide (FTO; 7 Ωsq^{-1}) glass substrate (TEC 7, Hartford, USA) to prepare the TiO_2 films (active area 0.4 × 0.4 cm^2, thickness ∼14 μm). A scattering layer (ST41, Ishihara Sangyo Kaisha, Japan, particle size ∼300 nm) with a thickness of ∼5 μm was added on top of the transparent active layer to enhance the performance of the NP based devices. The TiO_2 NP films were sensitized in a solution (Z907 dye, Everlight, 0.3 mM) containing chenodeoxycholic acid (CDCA, 0.3 mM) in acetonitrile/*t*-butanol (*v*/*v* = 1:1) binary solvent for 8 h. The TiNT films (0.4 × 0.4 cm^2) were sensitized by immersing them into a solution of N719 dye (3 × 10^{-4} M, Solaronix) containing chenodeoxycholic acid (CDCA, 3 × 10^{-4} M) in acetonitrile/tert-butanol (v/v = 1/1) binary solvent at room temperature for 18 h. The sensitized working electrodes were assembled with a Pt counter electrode and sealed with a hot-molten film (SX1170, Solaronix, thicknesses 25 and 60 μm for NP and NT based devices, respectively). The Pt counter electrode was

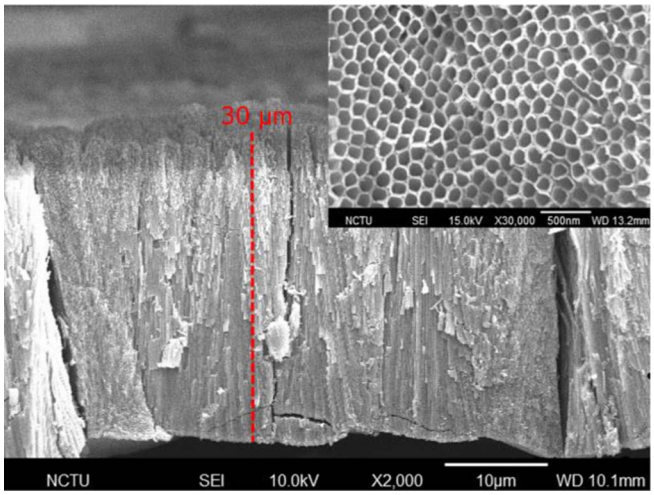

Figure 1. Side-view SEM image of the TiNT arrays with tube length (L) = 30 μm. The inset shows the SEM top-view image of the corresponding TiNT arrays.

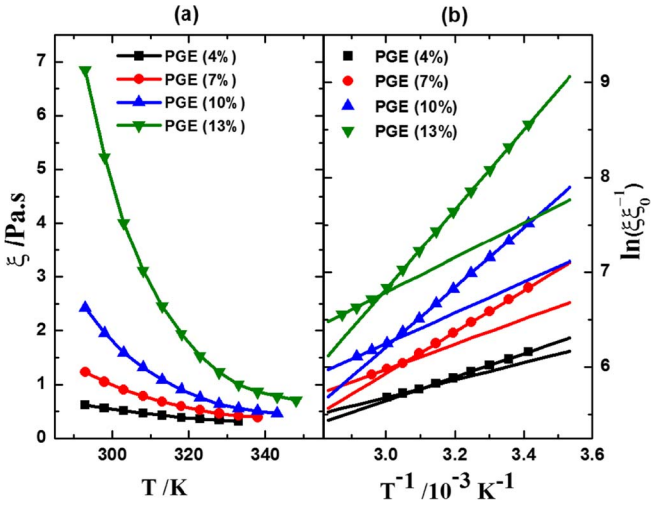

Figure 2. Plots of (a) viscosity (ξ) as a function of temperature (T) and (b) $\ln(\xi\xi_0^{-1})$ vs T^{-1} for electrolytes containing varied weight percentages of PMMA-EA copolymer in MPN.

prepared by spin coating a FTO substrate (typical size 1.0 × 1.5 cm^2) with the H_2PtCl_6/isopropanol solution and heating it at 380°C for 30 min.[29] To prepare gel-state device, hot liquid-state polymer electrolyte was introduced into a hole drilled in the counter electrode of the assembled cell, then the holes were sealed using a sealing spacer and a thin cover glass. To convert liquid-state polymer electrolyte to gel-state polymer electrolyte, the cells were sealed in two nested polyethylene bags (Ziploc) and stored at temperature about −4°C. Silver glue gel was coated on the counter electrode to enhance the electric conductivity.

Photovoltaic and impedance measurements.— The current-voltage characteristics were measured with a digital source meter (Keithley 2400, computer controlled). Photovoltaic measurements were carried out under 1 sun of illumination (AM-1.5G, 100 mW cm^{-2}) with a solar simulator (XES-40S1, SAN-EI) calibrated with a standard Si reference cell (VLSI standards, Oriel PN 91150 V). The efficiencies of conversion of incident photons to current (IPCE) of the devices were measured using a photoelectric spectral system composed of a Xe lamp (PTiA-1010, 150 W), a monochromator (PTi, 1200 gr mm^{-1} blazed at 500 nm), and a source meter (Keithley 2400). Back side illumination was used to characterize photovoltaic performance of the NT-DSSCs (active area 0.16 cm^2) for all measurements. Electrochemical impedance spectroscopy (EIS) measurements carried out using an electrochemical system (IM6, Zahner) were used to calculate the ionic conductivity and diffusion coefficient of the electrolytes. The EIS measurements of the electrolytes were performed using sandwich-type symmetric cells with a symmetrical configuration Pt/electrolyte/Pt. The frequency range was 0.01 Hz to 1 MHz, and the magnitude of the alternating potential was 20 mV. The EIS data were fitted to an equivalent circuit using simulation software (Z-view).

Results and Discussion

We produced anodic TiNT films with tube length (L) ∼30 μm at 22°C via anodization of Ti foil in the electrolyte solution at a constant voltage 60 V and an anodization period 12 h for use as a photoanode to fabricate gel-state NT-DSSCs. Figure 1 shows the SEM image of the TiNT arrays with L = 30 μm. The average pore diameter on top of the TiNT arrays is ∼100 nm, as shown in the inset of Figure 1. The as prepared TiNTs with $TiCl_4$-post treatment were sensitized with N719 dye and utilized to fabricate NT-DSSCs using the electrolytes containing varied concentrations of PMMA-EA copolymer. Properties of the PGEs containing various amounts of PMMA-EA in MPN were studied.

The viscosities of the PGEs containing varied concentrations of PMMA-EA in MPN measured at various temperatures are shown in Figure 2a. At the room temperature condition, the viscosity of the PGEs increased with increasing concentration of PMMA-EA. The viscosity of the PGEs exponentially decreased with increasing temperature. The data can be correlated via a simplified McAllister equation, $Ln(\xi/\xi_0) = Ln(B) + \frac{\Delta G^*}{RT}$, where ξ and ξ_0 are viscosities of polymer-containing and polymer-free electrolytes, respectively; ΔG^*, T, R and B represent the flow Gibbs energy, temperature, molar gas constant and pre-exponential factor, respectively.[38] ΔG^* means energy barrier against flow in a polymer electrolyte. Using the relationship between ξ and ΔG^* shown in Figure 2b, two Gibbs energy values of each PGE corresponding to the states of phase transition of the electrolytes were obtained. The phase transition temperature (T_p) of the PGEs is the temperature in which the phase state of the PGEs transforms from the gel-state with a higher viscosity and Gibbs energy to the liquid-state with a lower viscosity and Gibbs energy. The values of Gibbs energy calculated from the McAllister plot in both the gel (ΔG_g^*) and viscous liquid (ΔG_l^*) states and T_p values of PGEs containing various concentrations of PMMA-EA in MPN are listed in Table I. Our results

Table I. Flow Gibbs energy, phase transition temperature, ion diffusivity, ion conductivity and charge transfer resistance at the Pt/electrolyte interface of the electrolytes containing varied weight percentages of PMMA-EA copolymer in MPN.

PMMA-EA wt %	ΔG_l^*/kJ mol^{-1}	ΔG_g^*/kJ mol^{-1}	Temperature/K of phase transition	Diffusivity $D/10^{-6}$ cm^2 s^{-1}	Conductivity σ /mS cm^{-1}	R_{pt}/ Ω cm^2
0				4.1	1.7	2.8
4	7.6	10.3	322	3.8	1.5	3.4
7	11.0	18.1	328	3.5	1.4	3.9
10	13.5	26.2	331	3.4	1.6	3.0
13	15.2	34.9	335	1.1	1.2	3.8

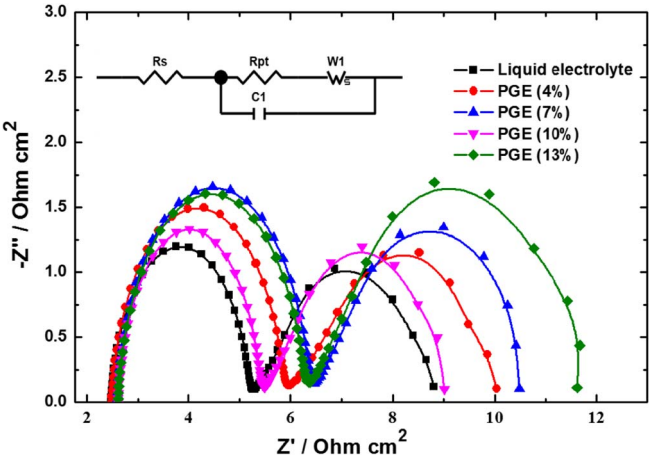

Figure 3. Nyquist plots of electrolytes containing varied weight percentages of PMMA-EA copolymer in MPN. Symbols demonstrate the measured EIS data and solid curves show the fitting results obtained from simulations based on the equivalent circuit model shown in the inset.

show a systematic trend for ΔG^* increasing with increasing concentration of PMMA-EA. The variation of T_p exhibited a similar trend, in which T_p increased from $T_p = 322$ K for the PGE containing 4 wt% PMMA-EA to $T_p = 335$ K for the PGE with 13 wt% PMMA-EA. The gelation time of the electrolytes decreased with increasing concentration of PMMA-EA. At temperature about −4°C, the gelation time was about 14 h when 4 wt% PMMA-EA was added to MPN and decreased to about 8, 4 and 2 h for electrolytes containing 7, 10 and 13 wt% PMMA-EA in MPN, respectively.

The ionic conductivity (σ/mS cm^{-1}) and diffusion coefficient (D/cm^2 s^{-1}) of each PGE were investigated using the EIS method. Figure 3 shows the Nyquist plots of sandwich-type symmetric cells composed of varied portions of PMMA-EA in MPN. The EIS data were fitted according to an equivalent circuit shown in the inset of Figure 3. As shown in Figure 3, only two semicircular characteristics were indicated in the plots: the first semicircles in the high-frequency domain represent the impedance of charge transfer at the Pt electrode/PGE interface and the second semicircles in the low-frequency domain reflect the contribution of Nernst diffusion in the gel electrolyte.[39] The diffusion coefficient D of tri-iodide ions in PGE can be determined via $D = (1/2.5)\, d^2 \omega_{max}$,[40] where d is the thickness of the electrolyte and ω_{max} is the peak frequency of the low frequency semicircle. To evaluate the influence of PMMA-EA addition on the charge transport, the conductivities of the PGEs were measured. The ionic conductivity σ is proportional to the diffusion resistant R_b via the relationship $\sigma = d/R_bA$, where d and A represent the thickness and the area of the PGE, respectively.

As shown in Table I, the diffusivity of tri-iodide decreased with increasing the concentration of PMMA-EA copolymer in MPN, and this trend is consistent with the trend of viscosities of the electrolytes showing an increasing feature upon increasing of concentration of PMMA-EA in MPN. The diffusivity of I_3^- was 4.1×10^{-6} cm^2 s^{-1} in the MPN liquid electrolyte, and decreased to 1.1×10^{-6} cm^2 s^{-1} in the PGE containing 13 wt% PMMA-EA in MPN. The conductivities of the electrolytes (σ) containing various amounts of PMMA-EA measured at near 23°C are also shown in Table I. The ionic conductivity σ of the polymer-free MPN-based liquid electrolyte was 1.7 mS cm^{-1}. The values of σ decreased to 1.5 and 1.4 mS cm^{-1} when 4 and 7 wt% of PMMA-EA were added, respectively. However, with further addition of PMMA-EA, the conductivity increased to attain maximum value of 1.6 mS cm^{-1} at 10 wt% but decreased on further increase. In general, the ionic conductivity of the electrolyte decreases upon increasing of concentration of PMMA-EA because of the retardation of the diffusion of the I_3^- ions in the presence of polymers. However, in our work, the effect of PMMA-EA addition on the ionic conductivity was not the same as its effect on the diffusivity. The observed enhancement of ionic conductivity in the PGE with certain portions of PMMA-EA is consistent with the phenomenon observed in the PAN-VA system,[41] and the charge exchange reaction ($I^- + I_3^- \rightarrow I_3^- + I^-$), i.e. Grotthus-type charge-transfer mechanism[35,42] was proposed for the I^-/I_3^- ion exchange reaction in the PGE having a conductivity similar to that in the polymer-free liquid electrolyte. When a lower concentration of PMMA-EA was added to the MPN-based liquid electrolyte, a large open structure derived from a poor connection of some polymer chains which leads to a decrease in ionic conductivity because of the delay of the diffusion of the I_3^- ions. With further increase of the amounts of PMMA-EA, the copolymer chains make contact with their neighbors to form a regular network including continuous pathways to reach an optimum condition. Figure 4 shows a Schematic illustration of ion transport, through a Grothus-type exchange mechanism, in a DSSC. It was reported that PMMA offers interactions with both ions and liquid components in addition to form a polymer network around liquid in PMMA-based gel electrolytes.[43] The solvation potential of PMMA-EA to cations increases the dissociation of LiI and PMII, leading to higher concentrations of I^- and I_3^-. Therefore higher amounts of I^-/I_3^- locates at the direct pathways associated with polymer network (Figure 4), leading to improved charge transport based on the exchange reaction. Although introducing the copolymer decreases the ion diffusion, increasing the exchange reaction leads to a higher conductivity. In other words, the reaction rates of ion exchange were enhanced in

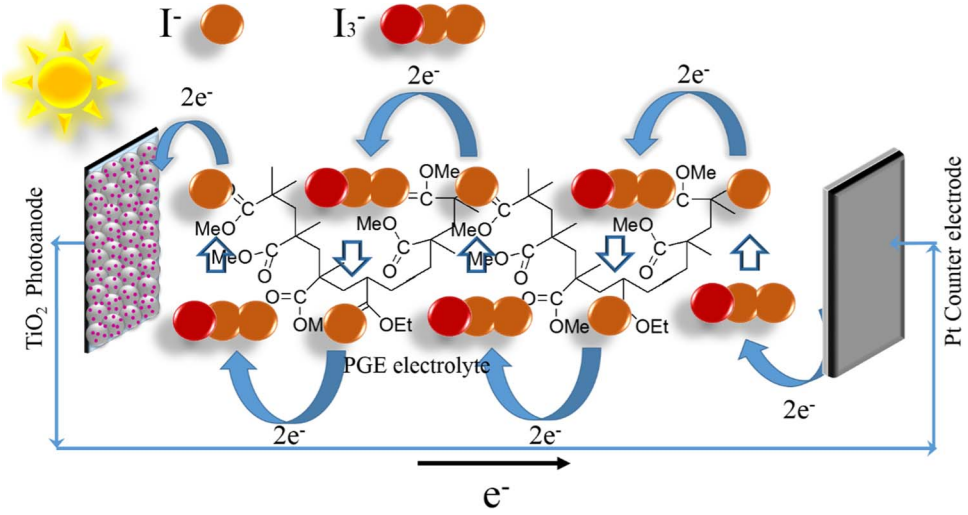

Figure 4. Schematic illustration of ion transport, through a Grothus-type exchange mechanism, in a NP-DSSC.

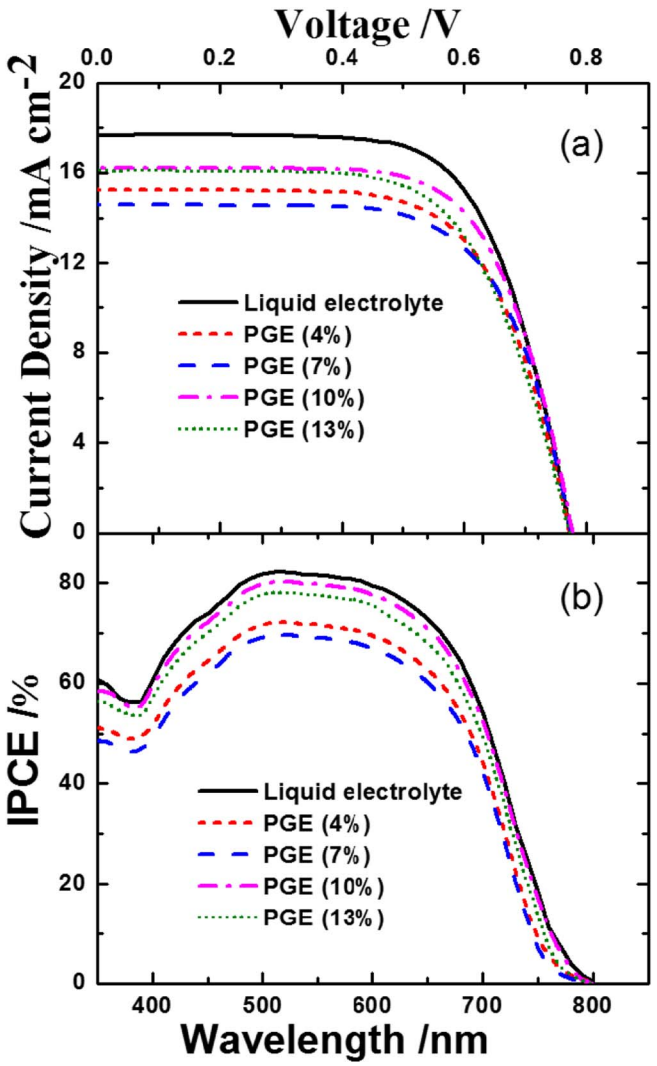

Figure 5. (a) Current-voltage characteristics and (b) IPCE action spectra of Z907-based NP-DSSC devices based on electrolytes containing varied weight percentages of PMMA-EA copolymer in MPN.

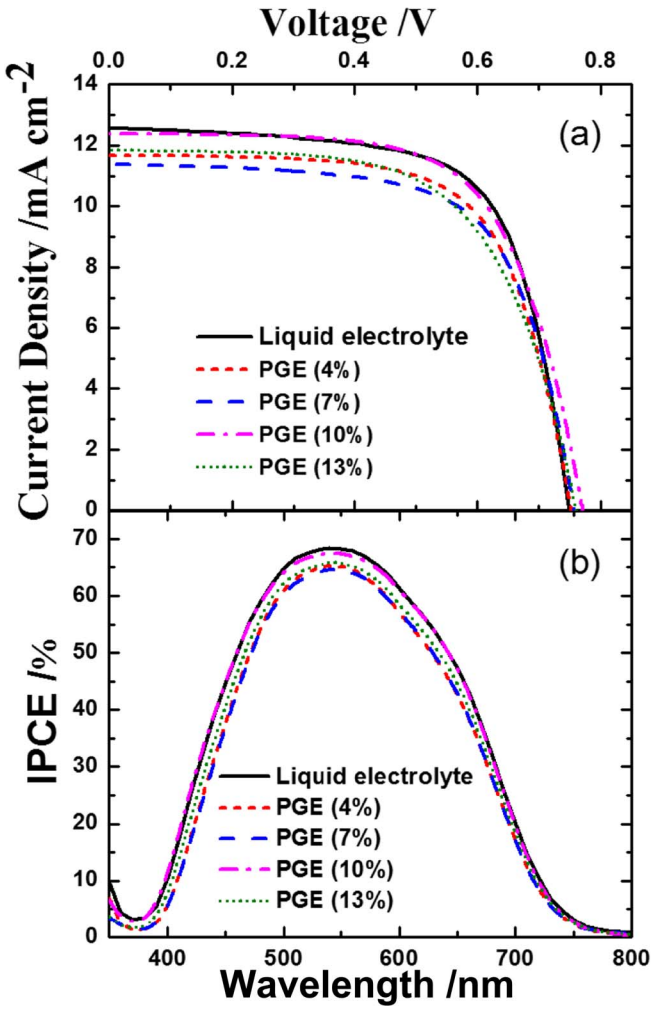

Figure 6. (a) Current-voltage characteristics and (b) IPCE action spectra of N719-based NT-DSSC devices with L = 30 μm based on electrolytes containing varied weight percentages of PMMA-EA copolymer in MPN.

PGE containing certain portions of PMMA-EA to compensate the increase of diffusion resistance caused by the polymer matrix. If we attain a higher concentration of the copolymer, aggregation occurs in the PGE as a result of the connection of polymer cages with each other and the effect of Grotthus charge transfer is diminished, leading to a decreased ionic transport. The charge transfer resistance at the Pt/electrolyte interface (R_{pt}) increased first up to 7 wt% addition of PMMA-EA, and then decreased on further addition of the copolymer to 10 wt%. However, further increase of PMMA-EA content in the electrolyte increased the R_{pt}. The charge transport resistance at the Pt surface is reported to increase with decreasing the roughness factor of the counter electrode.[44] We believe that the copolymer adsorbed onto the Pt counter may acts as a barrier against direct contact of the PGE to the counter electrode which suppresses the reduction of tri-iodide at the counter electrode, leading to an increased value of R_{pt}. However, at the optimal condition, the presence PMMA-EA increased the electroactivity of the Pt counter electrode, leading to a decrease in R_{pt}.

Figures 5a and 6a show typical *J-V* characteristics for the NP- and NT-based devices with electrolytes containing various amounts of PMMA-EA copolymer in MPN, respectively; the corresponding spectra of incident photon-to-current conversion efficiency (IPCE) were shown in Figures 5b and 6b, respectively. The corresponding photovoltaic parameters are summarized in Table II, giving the current density at short circuit (J_{SC}/mA cm^{-2}), voltage at open circuit (V_{OC}/mV), fill factor (*FF*), and efficiency ($\eta = J_{SC}V_{OC}FF / P_{in}$ with $P_{in} = 100$ mW cm^{-2}) of power conversion as a function of the copolymer concentration. The IPCE values of a back-illuminated NT-DSSC device were lower than those of its front-illuminated counterpart due to the loss of the incident light that result from the absorption of the I^-/I_3^- electrolyte and the light scattering of the Pt-FTO counter electrode.[29]

Table II. Photovoltaic parameters of the Z907-based NP-DSSCs and N719-based NT-DSSCs based on the electrolytes containing varied weight percentages of PMMA-EA copolymer in MPN under simulated AM-1.5 illumination (power 100 mW cm^{-2}) and active area 0.16 cm^2.

Systems	PMMA-EA /wt %	J_{SC}/mA cm^{-2}	V_{OC}/mV	FF	η/%
NP/Z907	0	17.54	774	0.667	9.1
	4	15.24	779	0.659	7.8
	7	14.60	773	0.670	7.6
	10	16.21	775	0.667	8.4
	13	16.04	772	0.653	8.1
NT/N719	0	12.56	748	0.678	6.4
	4	11.68	752	0.670	5.9
	7	11.37	757	0.665	5.7
	10	12.38	771	0.657	6.3
	13	11.86	760	0.626	5.6

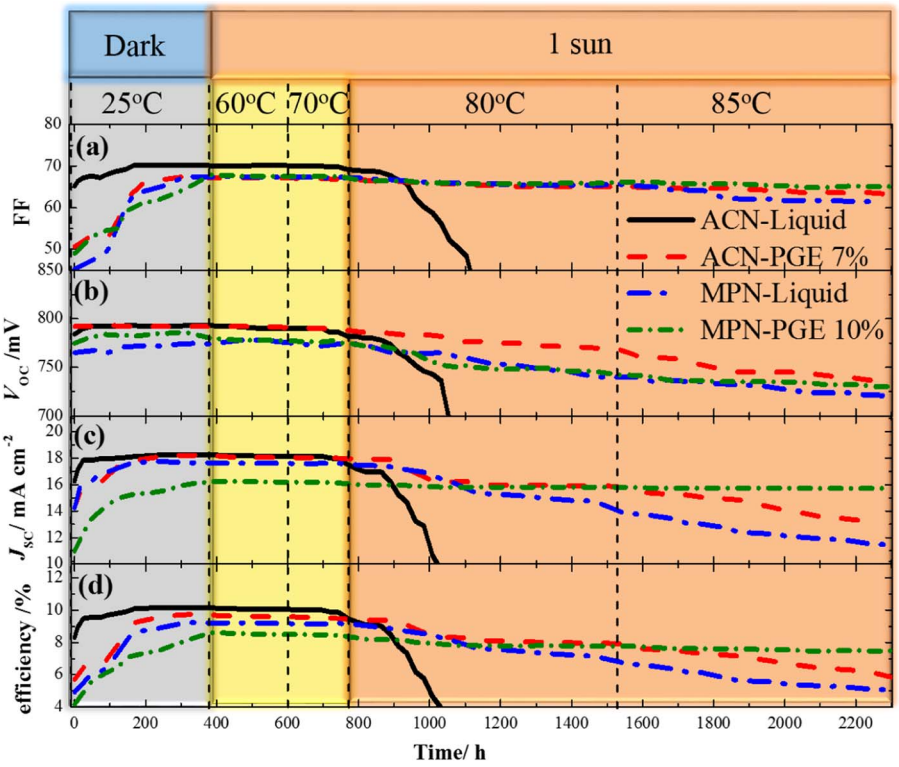

Figure 7. Enduring stability examination showing the variation of the photovoltaic performance for (a) fill factor (*FF*), (b) open-circuit voltage (V_{OC}), (c) short-circuit current density (J_{SC}) and (d) efficiency (η) of power conversion for the Z907-based NP-DSSC with ACN-liquid, ACN-PGE, MPN-liquid and MPN-PGE electrolyte systems. The experiments were carried out in dark at room temperature for 0–385 h, and then under one sun illumination during the periods 385–600 h at 60°C, 600–770 h at 70°C, 770–1540 h at 80°C and 1540–2300 h at 85°C.

For both NP and NT systems, J_{SC} of the cell decreased when up to 7 wt% of PMMA-EA was introduced to the liquid electrolyte. On further addition of the copolymer, J_{SC} increased first and then decreased after approaching a maximum value at 10 wt%, consistent with the variation of the ionic conductivity. For the NP/Z907 system, V_{OC} remained nearly constant with increasing concentration of the copolymer. It has been shown that for the NT-DSSC the presence of PMMA-EA up to 7 wt% in the ACN-based electrolyte increases V_{OC}.[35] For the NT/N719 system, V_{OC} of the device increased with increasing the copolymer concentration up to 10 wt%, and then decreased with any additional increase in concentration of the copolymer. For the NP-DSSC with 10 wt% PMMA-EA, the obtained efficiency was 8.4% which is 92% of the value measured for the MPN based liquid electrolyte (9.1%). The overall performance of NT-DSSC obtained using the MPN-based liquid electrolyte was PCE 6.4% (Table II). Due to relatively higher viscosity of MPN, performance of MPN-based liquid-type NT-DSSC was slightly poorer than that using the ACN-based electrolyte reported elsewhere.[28,35] For the NT-DSSC based on the PGE containing 10 wt% PMMA-EA, the cell performance was PCE 6.3%, which is 98% of the value obtained for the corresponding liquid-type device. We also showed *J-V* characteristics and IPCE action spectra of the NP-DSSC devices with electrolytes containing varied concentrations of PMMA-EA using ACN as solvent in Figures S1a and S1b, Supporting Information, respectively; the photovoltaic parameters are summarized in Table S1, Supporting Information. The best performance obtained using electrolyte contained 7 wt% PMMA-EA, consistent with our previous report.[35] The efficiency obtained for the NP-DSSC using PGE containing 7 wt% PMMA-EA in ACN was 9.6%,which was 95% of the value obtained for the liquid-based device (10.1%).

To study the effect of PGEs made of ACN and MPN solvents on the stability of the DSSCs, we selected one of the photoelectrodes. Because of the impressive performance of the gel state Z907-based NP-DSSC, we compared the performance of the NP-based device made of 10 wt% PMMA-EA in MPN with that contained 7 wt% PMMA-EA in the ACN-based PGE and without adding the copolymer in the MPN and ACN based liquid electrolytes under different experiment conditions over a period 2300 h to investigate the effect of MPN based PGE on the long-term stability of the DSSC device; The corresponding photovoltaic parameters as a function of light-soaking period are shown in Figure 7. In the first stage, the cells were kept in darkness at 25°C for 385 h. During this period, the performance of the devices increased and thereafter remained steady. For the second stage the cells were stored under one-sun illumination at 60°C during the period 385–600 h; the performance of the cells remained steady under this condition. Then the temperature of the cells was changed to 70°C under one-sun illumination during the period 600–770 h; the performance of the cell contained ACN based liquid electrolyte slightly decreased and other cells remained nearly constant. For the next stage we raised the temperature to 80°C under one-sun illumination during the period 770–1540 h; after about 880 h the device contained ACN based liquid electrolyte began to deteriorate and its performance degraded significantly after about 1000 h. Because the boiling point of the ACN is near 80°C, we predicted that the device contained ACN-based liquid electrolyte deteriorate under this condition. After 1360 h, the performance of devices made of 7 wt% PMMA-EA in the ACN-based PGE and polymer free MPN based liquid electrolyte decreased slightly but that of cell contained 10 wt% PMMA-EA remained nearly constant. For the final stage we increased the temperature of the cells to 85°C under one-sun irradiation during the period 1540–2300 h; the performance of the devices made of 7 wt% PMMA-EA in the ACN-based PGE and polymer free MPN-based liquid electrolyte degraded appreciably at 2300 h. Due to evaporation of the solvents under this condition, the J_{SC} of the devices decreased, which is the major factor responsible for the decreased efficiency of these devices. However the device contained 10 wt% PMMA-EA in the MPN-based PGE showed superior enduring stability and preserved PCE beyond 7.5% at the end of the test over 2000 h. We expect that (1) high boiling point of the MPN (~160°C) and (2) polymer cages in the electrolyte are responsible for the great enduring stability of the NP-DSSC device made of 10 wt% PMMA-EA in the electrolyte.

Conclusions

We have fabricated highly efficient gel-state DSSC devices using TiO_2 NPs and one-dimensional TiNT arrays as photoanodes.

PMMA-EA copolymer was used to solidify a MPN-based liquid electrolyte to obtain a new PGE for NP and NT based DSSCs. We used MPN instead of ACN to overcome the problem of high volatility of ACN and thus the long-term stability of the cells is enhanced. Using the viscosities measured at various temperatures, the phase transition temperature of the PGEs containing varied amounts of PMMA-EA (4–13 wt%) in MPN were obtained. The electrical conductivity (1.6 mS cm^{-1}) of the PGE containing 10 wt% of PMMA-EA in MPN was comparable to that (1.7 mS cm^{-1}) of the liquid electrolyte. NP- and NT-based DSSCs using this optimized PGE showed high power conversion efficiencies 8.4 and 6.3%, respectively, which are comparable to those of the corresponding MPN-based liquid-type devices. The continuous network formed by PMMA-EA along with the solvation ability of the copolymer to cations could also enhance the ionic conductivity of the PGE. Furthermore, the gel-state NP-DSSC with 10 wt% of PMMA-EA in MPN retained a high device performance for a long time over 2000 h under thermal stress and light soaking conditions.

Acknowledgments

We thank Dr. Hsiu-Ping Jen and Chien-Hung Shen for their assistance in this work at an initial stage. Ministry of Science and Technology (MOST) of Taiwan supported this work under the programs with the contract numbers NSC 102-2113-M-009-020-MY3, NSC 102-2622-M-009-001-CC1 and NSC 103-2623-E-009-001-ET. ZS thanks National Chiao Tung University (Hsinchu, Taiwan) and Iranian Ministry of Science and Technology (Tehran, Iran) for support of her visit to NCTU.

References

1. A. Hagfeldt, G. Boschloo, L. Sun, L. Kloo, and H. Pettersson, *Chem. Rev.*, **110**, 6595 (2010).
2. A. Hagfeldt and M. Grätzel, *Acc. Chem. Res.*, **33**, 269 (2000).
3. P. Wang, S. M. Zakeeruddin, J. E. Moser, M. K. Nazeeruddin, T. Sekiguchi, and M. Grätzel, *Nat. Mater.*, **2**, 402 (2003).
4. F. Fabregat-Santiago, J. Bisquert, L. Cevey, P. Chen, M. Wang, S. M. Zakeeruddin, and M. Grätzel, *J. Am. Chem. Soc.*, **131**, 558 (2009).
5. I. Chung, B. Lee, J. He, R. P. H. Chang, and M. G. Kanatzidis, *Nature*, **485**, 486 (2012).
6. J.-G. Chen, C.-Y. Chen, C.-G. Wu, and K.-C. Ho, *J. Phys. Chem. C*, **114**, 13832 (2010).
7. L.-Y. Chang, C.-P. Lee, R. Vittal, J.-J. Lin, and K.-C. Ho, *J. Mater. Chem. A*, **1**, 3055 (2013).
8. L. Tao, Z. Huo, Y. Ding, Y. Li, S. Dai, L. Wang, J. Zhu, X. Pan, B. Zhang, J. Yao, M. K. Nazeeruddin, and M. Grätzel, *J. Mater. Chem. A*, **3**, 2344 (2015).
9. J. N. de Freitas, A. F. Nogueira, and M.-A. De Paoli, *J. Mater. Chem.*, **19**, 5279 (2009).
10. Y. J. Kim, J. H. Kim, M.-S. Kang, M. J. Lee, J. Won, J. C. Lee, and Y. S. Kang, *Adv. Mater.*, **16**, 1753 (2004).
11. Y.-F. Chan, C.-C. Wang, and C.-Y. Chen, *J. Mater. Chem. A*, **1**, 5479 (2013).
12. H. Yang, M. Huang, J. Wu, Z. Lan, S. Hao, and J. Lin, *Mater. Chem. Phys.*, **110**, 38 (2008).
13. W. Xiang, W. Huang, U. Bach, and L. Spiccia, *Chem. Commun.*, **49**, 8997 (2013).
14. Z. Lan, J. Wu, J. Lin, M. Huang, and M. Polym. *Adv. Technol.*, **22**, 1812 (2011).
15. C.-L. Chen, T.-W. Chang, H. Teng, C.-G. Wu, C.-Y. Chen, Y.-M. Yang, and Y.-L. Lee, *Phys. Chem. Chem. Phys.*, **15**, 3640 (2013).
16. S. M. Zakeeruddin, Md. K. Nazeeruddin, R. Humphry-Baker, P. Péchy, P. Quagliotto, C. Barolo, G. Viscardi, and M. Grätzel, *Langmuir*, **18**, 952 (2002).
17. W.-K. Huang, C.-W. Cheng, S.-M. Chang, Y.-P. Lee, and E. W.-G. Diau, *Chem. Commun.*, **46**, 8992 (2010).
18. W.-K. Huang, H.-P. Wu, P.-L. Lin, Y.-P. Lee, and E. W.-G. Diau, *J. Phys. Chem. Lett.*, **3**, 1830 (2012).
19. W.-K. Huang, H.-P. Wu, P.-L. Lin, and E. W.-G. Diau, *J. Phys. Chem. C*, **117**, 2059 (2013).
20. J.-W. Shiu, C.-M. Lan, Y.-C. Chang, and H.-P. Wu , W.-K. Huang and E. W.-G. Diau, *ACS Nano*, **6**, 10862 (2012).
21. H.-P. Wu, C.-M Lan, J.-Y. Hu, W.-K. Huang, J.-W. Shiu, Z.-J. Lan, C.-M. Tsai, C.-H. Su, and E. W.-G. Diau, *J. Phys. Chem. Lett.*, **4**, 1570 (2013).
22. J.-W. Shiu, Z.-J. Lan, C.-Y. Chan, H.-P. Wu, and E. W.-G. Diau, *J. Mater. Chem. A*, **2**, 8749 (2014).
23. S. Venkatesan, S.-C. Su, S.-C. Kao, H. Teng, and Y.-L. Lee, *J. Power Sources*, **274**, 506 (2015).
24. D. Hwang, S. M. Jo, D. Y. Kim, V. Armel, D. R. MacFarlane, and S.-Y. Jang, *ACS Appl. Mater. Interfaces*, **3**, 1521 (2011).
25. J. B. Baxter and E. S. Aydil, *Appl. Phys. Lett.*, **86**, 053114 (2005).
26. K. Zhu, N. R. Neale, A. Miedaner, and A. J. Frank, *Nano Lett.*, **7**, 69 (2007).
27. K. Shankar, G. K. Mor, H. E. Prakasam, S. Yoriya, M. Paulose, O. K. Varghese, and C. A. Grimes, *Nanotechnology*, **18**, 065707 (2007).
28. C.-C. Chen, H.-W. Chung, C.-H. Chen, H.-P. Lu, C.-M. Lan, S.-F. Chen, L. Luo, C.-S. Hung, and E. W.-G. Diau, *J. Phys. Chem. C*, **112**, 19151 (2008).
29. L.-L. Li, C.-Y. Tsai, H.-P. Wu, C.-C. Chen, and E. W.-G. Diau, *J. Mater. Chem.*, **20**, 2753 (2010).
30. W. Sharmoukh and N. K. Allam, *ACS Appl. Mater. Interfaces*, **4**, 4413 (2012).
31. K. Lee, R. Kirchgeorg, and P. Schmuki, *J. Phys. Chem. C*, **118**, 16562 (2014).
32. S. H. Kang, J.-Y. Kim, Y. Kim, H. S. Kim, and Y.-E. Sung, *J. Phys. Chem. C*, **111**, 9614 (2007).
33. P. Chen, J. Brillet, H. Bala, P. Wang, S. M. Zakeeruddin, and M. Grätzel, *J. Mater. Chem.*, **19**, 5325 (2009).
34. I. C. Flores, J. N. de Freitas, C. Longo, M.-A. De Paoli, H. Winnischofer, and A. F. Nogueira, *J. Photochem. Photobiol., A*, **189**, 153 (2007).
35. Z. Seidalilir, R. Malekfar, H.-P. Wu, J.-W. Shiu, and E. W.-G. Diau, *ACS Appl. Mater. Interfaces*, **7**, 12731 (2015).
36. M. A. Ratner and D. F. Shriver, *Chem. Rev.*, **88**, 109 (1988).
37. G. B. Appetecchi, F. Croce, and B. Scrosati, *Electrochim. Acta*, **40**, 991 (1995).
38. J. Wu, S. Hao, Z. Lan, J. Lin, M. Huang, Y. Huang, L. Fang, S. Yin, and T. Sato, *Adv. Funct. Mater.*, **17**, 2645 (2007).
39. Q. Wang, J.-E. Moser, and M. Grätzel, *J. Phys. Chem. B*, **109**, 14945 (2005).
40. M. Adachi, M. Sakamoto, J. Jiu, Y. Ogata, and S. Isoda, *J. Phys. Chem. B*, **110**, 13872 (2006).
41. C.-L. Chen, H. Teng, and Y.-L. Lee, *J. Mater. Chem.*, **21**, 628 (2011).
42. R. Kawano and M. Watanabe, *Chem. Commun.*, 330 (2003).
43. C. S. Kim and S. M. Oh, *Electrochim. Acta*, **45**, 2101 (2000).
44. S. Zhang, X. Yang, Y. Numata, and L. Han, *Energy Environ. Sci.*, **6**, 1443 (2013).